Journal of Computational Applied Mechanics 2027, 58(1): 176-197

DOI: 10.22059/jcamech.2026.426019.2008

RESEARCH PAPER

Axisymmetric centrifugal response of a strain-gradient rotating nanodisk on a displacement-driven nonlocal elastic foundation

Worathep Sae-Long [a], Sutham Arun [b, *], Piti Sukontasukkul [c], Suchart Limkatanyu [d], Darrakorn Intarabut [e], Rut Su [c], Nattapong Damrongwiriyanupap [a], Chanachai Thongchom [f]

[a] *Civil Engineering Program, School of Engineering, University of Phayao, Phayao, 56000, Thailand*
[b] *Mechanical Engineering Program, School of Engineering, University of Phayao, Phayao, 56000, Thailand*
[c] *Construction and Building Materials Research Center, Department of Civil Engineering, King Mongkut's University of Technology North Bangkok, Bangkok, 10800, Thailand*
[d] *Department of Civil and Environmental Engineering, Faculty of Engineering, Prince of Songkla University, Songkhla, 90110, Thailand*
[e] *Department of Civil Engineering, Rajamangala University of Technology Phra Nakhon, Bangkok, 10800, Thailand*
[f] *Department of Civil Engineering, Faculty of Engineering, Thammasat School of Engineering, Thammasat University, Pathumthani, 12120, Thailand*

Abstract

This study develops an analytical framework for the axisymmetric centrifugal response of a rotating annular nanodisk interacting with a displacement-driven nonlocal elastic foundation. Small-scale material behavior is represented using a one-parameter simplified strain-gradient theory, whereas nonlocal substrate effects are introduced through a bi-exponential attenuation kernel. The governing sixth-order differential equation is obtained from the principle of virtual displacements and is completed by four mechanical and two foundation constitutive boundary conditions. The solution is expressed as a Frobenius-type series. Three numerical studies are then used to examine convergence, compare the classical limiting cases with finite element results, and evaluate the combined effects of material length scale, foundation nonlocality, and substrate stiffness. Convergence is achieved with 32 retained terms, while comparison with finite element solutions yields outer-radius displacement differences below 0.02%. The parametric results reveal competing size-dependent effects: increasing the material length-scale parameter reduces the radial displacement by up to 9.59%, whereas increasing the foundation nonlocal parameter increases it by up to 18.00%. Increasing the substrate stiffness reduces the displacement by 26.62% in the classical local limit. These results show that the material and foundation characteristic lengths exert distinct and competing influences and should therefore be treated independently when assessing the centrifugal response of rotating nanodisk–substrate systems.

Keywords: Rotating nanodisk; simplified strain-gradient elasticity; displacement-driven nonlocal foundation; elastic substrate medium; small-scale effect

1. Introduction

Rapid advances in nanotechnology have stimulated growing interest in miniaturized rotating components for

* Corresponding author. *E-mail address:* sutham.ar@up.ac.th

nanoelectromechanical and microelectromechanical systems (NEMS/MEMS), including nanogears, microgyroscopes, micromotors, miniature rotors, and disk-shaped resonating or sensing elements. At these scales, disk-like structures may undergo high-speed rotational motion while interacting with supporting surfaces or compliant surrounding media. For example, rotational transmission between a graphene nanodisk and a molecular gear has demonstrated the technological relevance of nanoscale disk rotation and substrate interaction [1], while studies of rotating microdisks and electromagnetic microdrives have highlighted their potential for microgyroscopic applications [2-4]. These developments motivate the formulation of reliable mechanical models capable of predicting centrifugal deformation and stress fields in rotating structures whose dimensions approach intrinsic material and interfacial length scales.

The mechanics of rotating micro- and nanodisks has consequently received considerable attention. Danesh and Asghari [5] developed a strain-gradient model for rotating microdisks and demonstrated the significance of small-scale effects on their mechanical response. Baghani et al. [6] subsequently investigated functionally graded rotating micro/nanodisks with variable thickness, while Hosseini et al. [7] presented a strain-gradient stress analysis of rotating functionally graded nanodisks with nonlinear thickness variation. [7] Thermomechanical and material-gradation effects were incorporated into related formulations in Shishesaz et al. [8] and Hosseini et al. [9]. Further extensions have addressed angular acceleration [10], thermal loading [11], variable rotational speed [12], piezoelectric coupling [13], multilayered rotating nanodisks interacting with viscoelastic media [14], and rotating shaft–disk systems described using nonlocal strain-gradient theories [15]. Collectively, these studies demonstrate that rotational speed, material length scales, geometry, thermal fields, and environmental restraint can interact strongly in determining the mechanical response of small-scale rotating structures.

The need for such enriched continuum descriptions originates from a fundamental limitation of classical elasticity: its constitutive equations contain no intrinsic material length scale and therefore cannot directly represent size-dependent elastic behavior. Higher-order continuum theories address this limitation by enriching the kinematic or constitutive description. Mindlin established general microstructural and first strain-gradient frameworks in which additional deformation measures and higher-order stresses arise [16, 17]. A particularly convenient simplification was proposed by Altan and Aifantis [18], in which the strain energy is augmented by strain-gradient contributions governed by a single intrinsic material length scale. Gradient concepts have subsequently been employed to describe experimentally observed size effects [19]. Other influential formulations include couple-stress-based gradient elasticity [20] and the modified strain-gradient theory of Lam et al. [21], which introduces multiple independent material length scales. Gao and Park [22] established a variationally consistent simplified strain-gradient formulation, while Askes and Aifantis [23] reviewed the theoretical basis, identification of characteristic length scales, and computational implementation of gradient elasticity.

An important advantage of simplified strain-gradient elasticity is that size-dependent stiffening can be represented without introducing the multiple higher-order constitutive parameters required by more general gradient theories. This feature has facilitated analytical and numerical studies of a wide range of micro- and nanostructures. Representative contributions include strain-gradient formulations for microbeams [24], one-dimensional gradient and nonlocal elasticity [25], simplified Bernoulli–Euler beam models [26], longitudinal vibration of microbars [27], and functionally graded microbeams resting on elastic foundations [28]. Nonlocal strain-gradient beam formulations have also been applied to free-vibration problems [29], while related higher-order theories have been developed for size-dependent bending, buckling, and wave propagation [30-32]. These studies indicate that higher-order material length scales can become mechanically significant when structural dimensions approach the intrinsic material length, making one-parameter strain-gradient formulations particularly attractive when analytical tractability is also required.

A second issue of comparable importance arises when a nanostructure interacts continuously with a supporting or surrounding medium. Nanoscale structural elements are frequently embedded in, deposited on, bonded to, or constrained by another material, and the resulting structure–substrate interaction can substantially modify their deformation and stress fields. Continuum foundation models provide an efficient representation of such interactions. Substrate effects have, for example, been incorporated into nanowire models accounting for nonlocality and surface energy [33] and into beam–substrate formulations employing enriched nanoscale mechanics [34-39]. Limkatanyu et al. [40] combined modified strain-gradient elasticity, surface elasticity, and a Winkler-type substrate to investigate the static and free-vibration response of single-walled carbon nanotube–substrate systems, while a related strain-gradient bar–substrate formulation was developed in Limkatanyu et al. [41]. Elastic-foundation effects have also been studied for piezoelectric nanobeams [42], thermally loaded nonhomogeneous nanobeams [43], and magneto-electro-elastic laminated nanobeams [44]. Recent investigations have also considered the combined influence of material length scales, surface energy, and substrate restraint on the mechanical response of nanobeams [45, 46]. In addition, Winkler-type foundation models can be derived as reduced representations of three-dimensional elastic substrates under suitable assumptions [47].

The conventional Winkler model relates the foundation reaction directly to the displacement at the same position. Although suitable for representing local elastic restraint, this assumption excludes the interaction between different regions of the supporting medium. Nonlocal elasticity provides one way of accounting for such interactions. The integral formulation introduced by Eringen and Edelen [48] established an important basis for subsequent nanoscale applications [49]. Its differential implementations, however, require care on bounded domains, where the choice of constitutive boundary conditions can affect the consistency of the solution [49-51]. Studies of spatially interacting beam foundations [52, 53] further indicate that the substrate response may depend on a characteristic interaction length in addition to the nominal foundation stiffness.

In the displacement-driven formulation of Vaccaro et al. [54], the foundation reaction is determined from a weighted distribution of structural displacement rather than from its value at a single point. The approach is particularly useful with a bi-exponential attenuation kernel because the integral constitutive law admits a differential representation. Two constitutive boundary conditions are then required to preserve equivalence with the original integral relation. These conditions are not mechanical constraints on the supported structure; they specify the behavior of the nonlocal reaction field at the ends of the interaction interval [54, 55].

The preceding literature points to two comparatively well-developed but largely distinct lines of research. The first concerns size-dependent rotating micro- and nanodisks formulated within strain-gradient, nonlocal strain-gradient, and related higher-order continuum theories [5, 6, 15]. These studies have clarified the effects of intrinsic material length scales, material gradation, thickness variation, thermal loading, and rotational parameters on the disk response. However, the surrounding medium is generally either neglected or represented through conventional local interactions. The second line concerns nanobars and nanobeams interacting with elastic substrates [33, 38, 52-54], where increasingly sophisticated descriptions of bulk nonlocality, surface energy and foundation behaviour have been introduced. In particular, displacement-driven nonlocal foundation theory offers a mathematically consistent means of representing spatial interaction within the supporting medium [54, 55]. Nevertheless, the literature considered here does not reveal an analytical formulation that combines a strain-gradient rotating annular nanodisk with a displacement-driven nonlocal radial elastic foundation. The consequences of simultaneously introducing an intrinsic material length scale in the nanodisk and an independent nonlocal interaction length in the substrate therefore remain insufficiently understood.

The present study addresses this gap by developing a displacement-based analytical formulation for the axisymmetric centrifugal response of a thin rotating annular nanodisk continuously interacting with a displacement-driven nonlocal elastic foundation. The material small-scale effect of the nanodisk is represented by the one-parameter simplified strain-gradient elasticity model [18, 22], whereas spatial interaction within the substrate is described through the displacement-driven nonlocal foundation concept [54]. The formulation is established under infinitesimal deformation, plane-stress and axisymmetric conditions, with the radial displacement adopted as the sole primary kinematic field. To preserve analytical tractability, only the radial gradients of the radial and circumferential strains are retained, so that the model should be interpreted as a mono-dimensional radial strain-gradient approximation rather than a complete three-dimensional cylindrical strain-gradient theory. The displacement-driven foundation concept, originally developed for beam–foundation systems, is extended here to the radial interaction domain of an annular nanodisk.

Application of the principle of virtual displacements first yields the fourth-order mechanical equilibrium equation associated with the strain-gradient nanodisk, while the substrate reaction is retained as an independently governed constitutive field. Combining this equilibrium relation with the differential representation of the displacement-driven nonlocal foundation reduces the coupled problem to a single sixth-order nonhomogeneous differential equation in the radial displacement. The resulting boundary-value problem contains four mechanical conditions associated with the classical and higher-order nanodisk tractions and two foundation constitutive boundary conditions inherited from the nonlocal substrate law. This separation is essential because the latter conditions do not represent mechanical edge forces or displacements. The general displacement solution is subsequently decomposed into homogeneous and particular components, providing an analytical basis for evaluating the competing influences of material strain-gradient stiffening, substrate stiffness, foundation nonlocality and centrifugal loading.

The principal contribution of the present study is therefore the simultaneous treatment of internal material small-scale behaviour and external substrate nonlocality through two physically distinct characteristic lengths. Unlike a local Winkler-supported strain-gradient disk, the present formulation allows the substrate reaction at a given radial position to depend on the displacement field over the complete interaction interval. Conversely, unlike a purely nonlocal structural model, the material size effect remains governed by strain-gradient energetics and its associated higher-order mechanical boundary conditions. The formulation also provides transparent limiting connections to local-foundation and classical-elasticity models as the relevant characteristic lengths vanish. The resulting framework is intended to provide a basis for analysing substrate-constrained rotating nanostructures and for

subsequent extensions involving material gradation, thermal fields, surface elasticity, damage, variable thickness and more general nonlocal substrate models.

2. Method

The present study develops a displacement-based analytical formulation for the axisymmetric centrifugal response of a thin rotating annular nanodisk interacting continuously with an elastic substrate medium. The size-dependent behavior of the nanodisk is described using one-parameter simplified strain-gradient elasticity, while the substrate interaction is represented by a displacement-driven nonlocal foundation characterized by the foundation stiffness (k_s) and the nonlocal interaction length (l_s). Under the assumptions of infinitesimal deformation, plane stress, and axisymmetric motion, the radial displacement ($U\left(r\right)$) is adopted as the primary field variable. The governing equilibrium equation and the associated mechanical boundary conditions are derived from the principle of virtual displacements. The differential constitutive relation of the nonlocal foundation is then combined with the nanodisk equilibrium equation to obtain a single sixth-order differential equation in $U\left(r\right)$. The resulting boundary-value problem is supplemented by four mechanical boundary conditions associated with the nanodisk and two constitutive boundary conditions arising from the nonlocal foundation model. The displacement solution is subsequently decomposed into homogeneous and particular components to facilitate the analytical treatment of the governing equation.

2.1. Simplified strain-gradient elasticity of the rotating nanodisk

Classical continuum elasticity describes the mechanical response of an elastic solid using a strain-energy density that depends only on the conventional strain field. As a result, the classical constitutive framework contains no intrinsic material length-scale parameter and predicts scale-independent elastic behaviour. This assumption becomes increasingly restrictive when the characteristic dimensions of a structural component approach the internal length associated with the underlying material microstructure. To account for the resulting small-scale effect while preserving analytical tractability, the present study adopts the one-parameter simplified strain-gradient elasticity model proposed by Altan and Aifantis [18] and later established within a variational framework. In this model, the strain-energy density is enriched by the spatial gradients of the conventional strain field, thereby introducing an intrinsic material length-scale parameter into the constitutive description. The adopted formulation is therefore consistent with the simplified strain-gradient framework previously used for axisymmetric rotating nanodisks. Under the infinitesimal-deformation assumption, the conventional strain tensor (ε_{ij}) of an elastic continuum is defined as:

$$\varepsilon_{ij} = \frac{1}{2}\left(u_{i,j} + u_{j,i}\right) \tag{1}$$

where u_i denotes the displacement tensor.

The associated first strain-gradient tensor (η_{ijk}) is defined as:

$$\eta_{ijk} = \varepsilon_{ij,k} \tag{2}$$

For a homogeneous, isotropic, linearly elastic material, the strain-energy density of the one-parameter simplified strain-gradient elastic solid is expressed as:

$$W = \frac{1}{2}C_{ijkl}\varepsilon_{ij}\varepsilon_{kl} + \frac{l_c^2}{2}C_{ijkl}\varepsilon_{ij,m}\varepsilon_{kl,m} \tag{3}$$

where C_{ijkl} is the fourth-order classical elasticity tensor; and l_c denotes the intrinsic material length-scale parameter. The first term in Eq. (3) represents the conventional elastic strain energy, whereas the second term represents the additional energy associated with spatial variations of the strain field. Hence, the relative importance of the strain-gradient effect is governed by the ratio between l_c and a characteristic dimension of the nanodisk. As this ratio tends

to zero, the strain-gradient contribution progressively vanishes and the classical elastic response is recovered.

The stress measures energetically conjugate to the conventional strain field and its gradient are the Cauchy stress tensor (σ_{ij}) and the third-order double-stress tensor (μ_{ijm}), respectively. From the strain-energy density in Eq. (3), these stress measures are obtained as:

$$\sigma_{ij} = \frac{\partial W}{\partial \varepsilon_{ij}} = C_{ijkl}\varepsilon_{kl} \tag{4}$$

$$\mu_{ijm} = \frac{\partial W}{\partial \varepsilon_{ij,m}} = l_c^2 C_{ijkl}\varepsilon_{kl,m} \tag{5}$$

The double stress has the physical dimension of conventional stress multiplied by length and represents the energetic resistance associated with spatial variation of the strain field. Its presence increases the differential order of the resulting structural formulation and consequently introduces higher-order boundary conditions in addition to the classical mechanical boundary conditions. The formulation adopted herein therefore differs from multi-parameter modified strain-gradient models, such as the Lam-type theory, in which several independent material length-scale parameters are associated with different higher-order deformation modes. The present model employs only the single parameter (l_c), which captures the essential strain-gradient effect while preserving analytical tractability.

2.2. Displacement-driven nonlocal elastic substrate

The mechanical interaction between a nanostructure and its surrounding substrate is commonly represented using the Winkler foundation model. In its classical local form, the substrate is idealized as a continuous distribution of mutually independent elastic springs, such that the reaction developed at a given material point depends only on the displacement at the same point. For the axisymmetric rotating nanodisk considered herein, this concept is adapted to the in-plane radial direction, where the substrate reaction opposes the centrifugal expansion of the nanodisk. A radial Winkler-type representation has previously been adopted for substrate-constrained rotating annular nanodisks. Although this local foundation model provides a convenient description of substrate restraint, it does not capture spatial interactions between neighboring regions of the supporting medium. In an actual continuous substrate, deformation imposed at one location may influence the reactions developed at surrounding locations. To incorporate this spatial interaction while retaining a tractable one-dimensional formulation, the present study adopts the displacement-driven nonlocal foundation concept proposed by Vaccaro et al. [54]. In this approach, the foundation reaction is treated as the output of a spatial convolution between the structural displacement field and an attenuation kernel. For a bi-exponential kernel, the corresponding integral constitutive relation admits an equivalent differential representation supplemented by two foundation constitutive boundary conditions. It should be emphasized that the displacement-driven nonlocal foundation was originally formulated for beam–foundation systems. In the present study, this concept is extended to the axisymmetric radial interaction between an annular nanodisk and its surrounding elastic medium. Accordingly, the formulation introduced below represents a one-dimensional radial adaptation of the displacement-driven nonlocal foundation, rather than a complete two-dimensional nonlocal description of the substrate.

Based on the displacement-driven nonlocal foundation concept, the radial substrate reaction ($D_s\left(r\right)$) acting on the nanodisk is expressed through the following convolution integral:

$$D_s\left(r\right) = \int_{r_0}^{r_i} \phi\left(r-\xi, l_s\right) k_s U\left(\xi\right) d\xi \tag{6}$$

where ξ is the integration coordinate; and l_s denotes the characteristic length associated with nonlocal interaction within the substrate medium [54].

Following the displacement-driven nonlocal foundation theory, the attenuation kernel is adopted in the following bi-exponential form:

$$\phi\left(r-\xi,l_s\right)=\frac{1}{2l_s}\exp\left(-\frac{\left|r-\xi\right|}{l_s}\right) \tag{7}$$

The displacement-driven character of Eq. (6) should also be emphasized. The radial displacement ($U\left(\xi\right)$) serves as the input field, whereas $D_s\left(r\right)$ is the resulting nonlocal substrate-reaction field. This input–output ordering distinguishes the present model from reaction-driven nonlocal foundation formulations, in which the displacement is instead expressed as an integral functional of the foundation reaction field. The displacement-driven strategy was introduced specifically to obtain a well-posed nonlocal foundation formulation without requiring fictitious concentrated reactions at the boundaries.

Direct treatment of the convolution integral in Eq. (6) would result in an integro-differential formulation when coupled with the equilibrium equation of the rotating nanodisk. However, a key property of the bi-exponential kernel in Eq. (7) is that the displacement-driven integral law can be transformed into an equivalent ordinary differential constitutive equation. Adapting this equivalence property, originally established for displacement-driven nonlocal foundations, to the radial interval [r_0, r_1], Eq. (6) is recast as:

$$D_s\left(r\right)-l_s^2\frac{d^2D_s\left(r\right)}{dr^2}=k_sU\left(r\right) \tag{8}$$

Equation (8) highlights the difference between the present nonlocal foundation and the conventional Winkler model. For a local foundation, the substrate reaction depends algebraically on the local displacement ($U\left(r\right)$), whereas the displacement-driven nonlocal foundation introduces the second radial derivative of $D_s\left(r\right)$. Consequently, the substrate reaction becomes an additional spatially varying field governed by its own differential constitutive equation. For completeness, Eq. (8) can also be rearranged to express the radial displacement of the disk in terms of the substrate reaction as:

$$U\left(r\right)=\frac{1}{k_s}\left(D_s\left(r\right)-l_s^2\frac{d^2D_s\left(r\right)}{dr^2}\right) \tag{9}$$

The differential constitutive relation in Eq. (8) is not, by itself, equivalent to the original convolution law in Eq. (6) unless it is supplemented by appropriate foundation constitutive boundary conditions. For the radial interaction interval [r_0, r_1], the corresponding conditions are obtained by adapting the displacement-driven foundation boundary conditions to the annular radial domain.

At the inner interaction boundary: $r=r_0$

$$\left[\frac{dD_s\left(r\right)}{dr}-\frac{1}{l_s}D_s\left(r\right)\right]_{r=r_0}=0 \tag{10}$$

At the outer interaction boundary: $r=r_1$

$$\left[\frac{dD_s\left(r\right)}{dr}+\frac{1}{l_s}D_s\left(r\right)\right]_{r=r_1}=0 \tag{11}$$

These relations are referred to herein as the foundation constitutive boundary conditions (FBCs). They arise from the nonlocal constitutive description of the substrate and are therefore conceptually distinct from the mechanical boundary conditions associated with the nanodisk itself. In particular, they should not be interpreted as prescribed

radial forces, prescribed displacements, conventional tractions, or higher-order tractions applied at the disk edges. This distinction becomes essential in the coupled formulation developed in the following section.

2.3. Displacement-based formulation

A thin annular nanodisk occupying the radial domain $[r_0,\ r_1]$ is considered. The nanodisk undergoes infinitesimal, axisymmetric, in-plane deformation while rotating with a prescribed constant angular velocity (ω). Owing to the axisymmetry of the geometry and centrifugal loading, the displacement field is represented solely by the radial displacement component and is expressed as:

$$u_r\left(r\right)=U\left(r\right) \quad ;\ u_\theta\left(r\right)=0\ ; \qquad \text{and } u_z\left(r\right)=0 \tag{12}$$

where $u_r\left(r\right)$, $u_\theta\left(r\right)$, and $u_z\left(r\right)$ denote the radial, circumferential, and axial displacement components.

2.3.1. Compatibility relations

Under the infinitesimal-deformation assumption, the corresponding nonzero in-plane strain components ($\varepsilon_{rr}\left(r\right)$ and $\varepsilon_{\theta\theta}\left(r\right)$) are expressed as:

$$\varepsilon_{rr}\left(r\right)=\frac{dU\left(r\right)}{dr} \tag{13}$$

$$\varepsilon_{\theta\theta}\left(r\right)=\frac{U\left(r\right)}{r} \tag{14}$$

Because the nanodisk is thin compared with its in-plane dimensions, the classical elastic response is described under the plane-stress condition. Accordingly, the out-of-plane normal stress is neglected, while the shear stress components vanish in the present axisymmetric radial formulation. It should be noted that the angular velocity (ω) does not explicitly enter Eqs. (12)–(14). Rotation provides the centrifugal body force acting on the nanodisk and therefore enters the equilibrium or variational formulation developed subsequently, whereas the strain–displacement and constitutive relations remain determined by the radial displacement field ($U\left(r\right)$).

To retain an analytically tractable formulation, the present study adopts a one-dimensional radial reduction of the simplified strain-gradient model. Specifically, only the radial derivatives of the two nonzero in-plane strain components, $\varepsilon_{rr}\left(r\right)$ and $\varepsilon_{\theta\theta}\left(r\right)$, are retained. The active strain-gradient components ($\eta_{rrr}\left(r\right)$ and $\eta_{\theta\theta r}\left(r\right)$) are therefore expressed as:

$$\eta_{rrr}\left(r\right)=\frac{d\varepsilon_{rr}\left(r\right)}{dr}=\frac{d^2U\left(r\right)}{dr^2} \tag{15}$$

$$\eta_{\theta\theta r}\left(r\right)=\frac{d\varepsilon_{\theta\theta}\left(r\right)}{dr}=\frac{1}{r}\frac{dU\left(r\right)}{dr}-\frac{U\left(r\right)}{r^2} \tag{16}$$

This reduction is deliberately introduced to describe the radial variation of the in-plane strain field governing the axisymmetric radial deformation of the nanodisk under centrifugal loading. In a complete three-dimensional strain-gradient formulation expressed in cylindrical coordinates, additional covariant-gradient components may arise because of the spatial variation of the cylindrical basis vectors. These components are not retained in the present formulation. Consequently, Eqs. (15) and (16) should be interpreted as a one-dimensional radial strain-gradient approximation, rather than as a complete three-dimensional cylindrical strain-gradient representation. This distinction was explicitly recognized in the preceding rotating-nanodisk formulation and is retained here to avoid overinterpreting the reduced model. The adopted reduction has an important practical advantage. Since both strain-gradient measures are expressed entirely in terms of $U\left(r\right)$ and its radial derivatives, the complete nanodisk problem

can subsequently be formulated using the radial displacement as the sole primary kinematic variable.

2.3.2. Cauchy and double-stress relations

Under the plane-stress condition, the conventional radial and circumferential stress components ($\sigma_{rr}\left(r\right)$ and $\sigma_{\theta\theta}\left(r\right)$) are expressed from Eq. (4) as:

$$\sigma_{rr}\left(r\right)=\frac{E}{1-\nu^2}\left[\varepsilon_{rr}\left(r\right)+\nu\varepsilon_{\theta\theta}\left(r\right)\right] \tag{17}$$

$$\sigma_{\theta\theta}\left(r\right)=\frac{E}{1-\nu^2}\left[\varepsilon_{\theta\theta}\left(r\right)+\nu\varepsilon_{rr}\left(r\right)\right] \tag{18}$$

where E and ν denote the Young's modulus and Poisson's ratio, respectively.

Similarly, the nonzero double-stress components ($\mu_{rrr}\left(r\right)$ and $\mu_{\theta\theta r}\left(r\right)$) associated with the one-dimensional radial strain-gradient measures are obtained as:

$$\mu_{rrr}\left(r\right)=\frac{El_c^2}{1-\nu^2}\left[\eta_{rrr}\left(r\right)+\nu\eta_{\theta\theta r}\left(r\right)\right] \tag{19}$$

$$\mu_{\theta\theta r}\left(r\right)=\frac{El_c^2}{1-\nu^2}\left[\eta_{\theta\theta r}\left(r\right)+\nu\eta_{rrr}\left(r\right)\right] \tag{20}$$

Substituting Eqs. (13) and (14) into Eqs. (17) and (18) yields the conventional stress–displacement relations:

$$\sigma_{rr}\left(r\right)=\frac{E}{1-\nu^2}\left[\frac{dU\left(r\right)}{dr}+\nu\frac{U\left(r\right)}{r}\right] \tag{21}$$

$$\sigma_{\theta\theta}\left(r\right)=\frac{E}{1-\nu^2}\left[\frac{U\left(r\right)}{r}+\nu\frac{dU\left(r\right)}{dr}\right] \tag{22}$$

Likewise, substituting Eqs. (15) and (16) into Eqs. (19) and (20) yields the double-stress components expressed in terms of the radial displacement:

$$\mu_{rrr}\left(r\right)=\frac{El_c^2}{1-\nu^2}\left[\frac{d^2U\left(r\right)}{dr^2}+\nu\left(\frac{1}{r}\frac{dU\left(r\right)}{dr}-\frac{U\left(r\right)}{r^2}\right)\right] \tag{23}$$

$$\mu_{\theta\theta r}\left(r\right)=\frac{El_c^2}{1-\nu^2}\left[\frac{1}{r}\frac{dU\left(r\right)}{dr}-\frac{U\left(r\right)}{r^2}+\nu\frac{d^2U\left(r\right)}{dr^2}\right] \tag{24}$$

These relations establish the constitutive description required for the subsequent displacement-based formulation. The Cauchy stresses depend on $U\left(r\right)$ and its first derivative, whereas the double stresses additionally depend on the second derivative of the radial displacement. Consequently, incorporating the strain-gradient contribution into the variational equilibrium equation produces a fourth-order differential operator in terms of $U\left(r\right)$. In the present study, this intrinsic higher-order nanodisk response is subsequently coupled with the displacement-driven nonlocal foundation behaviour of the elastic substrate.

2.3.3. Principle of virtual displacements

As presented in Figure 1, the mechanical response of the rotating nanodisk–substrate system is formulated using the radial displacement as the primary kinematic field. The conventional strain components and the one-dimensional radial strain-gradient measures are therefore determined directly from the compatibility relations introduced in Section 2.3.1, whereas mechanical equilibrium is imposed in a weak sense through the principle of virtual displacements. A key feature of the present formulation is that the substrate reaction is retained as a constitutively governed field during the equilibrium derivation. Unlike the classical radial Winkler model, no pointwise substitution of the form of $D_s\left(r\right)=k_sU\left(r\right)$ is introduced at this stage. Instead, the substrate reaction is governed separately by the displacement-driven nonlocal constitutive relation established in Section 2.2. This separation preserves a clear distinction between the mechanical equilibrium of the strain-gradient nanodisk and the spatially nonlocal foundation behaviour of the surrounding substrate. For an admissible virtual radial displacement ($\delta U\left(r\right)$), the principle of virtual displacements requires:

$$\delta W=\delta W_{\text{int}}+\delta W_{\text{ext}}=0 \tag{25}$$

where δW , δW_{int} , and δW_{ext} denote the total, internal, and external virtual work.

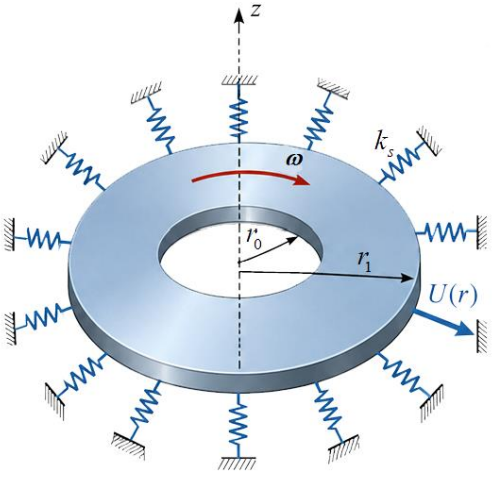


Fig 1: A rotating nanodisk–substrate system

For the one-dimensional radial strain-gradient formulation adopted in this study, the internal virtual work of the nanodisk in an elastic substrate medium is expressed as:

$$\begin{aligned}\delta W_{\text{int}}&=2\pi h\int_{r_0}^{r_1}\left(\sigma_{rr}\left(r\right)\delta\varepsilon_{rr}\left(r\right)+\sigma_{\theta\theta}\left(r\right)\delta\varepsilon_{\theta\theta}\left(r\right)+\mu_{rrr}\left(r\right)\delta\eta_{rrr}\left(r\right)\right)rdr\\&+2\pi h\int_{r_0}^{r_1}\left(\mu_{\theta\theta r}\left(r\right)\delta\eta_{\theta\theta r}\left(r\right)+D_s\left(r\right)\delta U\left(r\right)\right)rdr\end{aligned} \tag{26}$$

where h denotes the constant nanodisk thickness.

The external virtual work of the nanodisk can be written as:

$$\delta W_{\text{ext}}=-2\pi h\int_{r_0}^{r_1}\rho\omega^2r^2\delta U\left(r\right)dr-\delta\mathbf{U}^{\mathbf{T}}\mathbf{P} \tag{27}$$

where ρ denotes the mass density of the nanodisk; $\mathbf{U}$ and $\mathbf{P}$ denotes the displacement and force vector.

Substituting Eqs. (13)–(16) into Eqs. (26) and (27), and then substituting the resulting expressions into Eq. (25), yields the displacement-based weak form:

$$\delta W = 2\pi h \int_{r_0}^{r_1} \left[\begin{array}{l} r\mu_{rrr}\left(r\right)\dfrac{d^2\delta U\left(r\right)}{dr^2} + \left(r\sigma_{rr}\left(r\right) + \mu_{\theta\theta r}\left(r\right)\right)\dfrac{d\delta U\left(r\right)}{dr} \\ + \left(\sigma_{\theta\theta}\left(r\right) - \dfrac{\mu_{\theta\theta r}\left(r\right)}{r} + rD_s\left(r\right) - \rho\omega^2 r^2\right)\delta U\left(r\right) \end{array} \right] dr - \delta\mathbf{U}^{\mathbf{T}}\mathbf{P} = 0 \tag{28}$$

Equation (28) constitutes the fundamental weak form of the present rotating nanodisk–substrate system. The first two terms represent the strain-gradient and conventional elastic contributions of the nanodisk, respectively, whereas the remaining terms include the circumferential stress contribution, the nonlocal substrate reaction, and the centrifugal loading. The substrate nonlocality does not modify the kinematic structure of the weak form; rather, it enters through the constitutive determination of the substrate-reaction field.

2.3.4. Governing equilibrium equation

To derive the strong-form equilibrium equation, integration by parts is applied twice to the term in Eq. (28), resulting in the following expression.

$$\begin{aligned} \delta W = {} & 2\pi h \int_{r_0}^{r_1} \delta U\left(r\right) \left[\begin{array}{l} \dfrac{d^2}{dr^2}\left(r\mu_{rrr}\left(r\right)\right) - \dfrac{d}{dr}\left(r\sigma_{rr}\left(r\right) + \mu_{\theta\theta r}\left(r\right)\right) \\ + \sigma_{\theta\theta}\left(r\right) - \dfrac{\mu_{\theta\theta r}\left(r\right)}{r} + rD_s\left(r\right) - \rho\omega^2 r^2 \end{array} \right] dr - \delta\mathbf{U}^{\mathbf{T}}\mathbf{P} \\ & + 2\pi h \left[\delta U\left(r\right)\left(r\sigma_{rr}\left(r\right) + \mu_{\theta\theta r}\left(r\right) - \frac{d}{dr}\left(r\mu_{rrr}\left(r\right)\right)\right)\right]_{r=r_0}^{r=r_1} \\ & + 2\pi h \left[\frac{d\delta U\left(r\right)}{dr}\left(r\mu_{rrr}\left(r\right)\right)\right]_{r=r_0}^{r=r_1} = 0 \end{aligned} \tag{29}$$

Because the virtual displacement ($\delta U\left(r\right)$) is arbitrary over the open radial interval $r_0 \le r \le r_1$, localization of the weak form in Eq. (29) yields the strong-form radial equilibrium equation.

$$\frac{d^2}{dr^2}\left(r\mu_{rrr}\left(r\right)\right) - \frac{d}{dr}\left(r\sigma_{rr}\left(r\right) + \mu_{\theta\theta r}\left(r\right)\right) + \sigma_{\theta\theta}\left(r\right) - \frac{\mu_{\theta\theta r}\left(r\right)}{r} + rD_s\left(r\right) = \rho\omega^2 r^2 \tag{30}$$

By substituting the stress–displacement relations in Eqs. (21)–(24) and the foundation constitutive relation in Eq. (8) into the radial equilibrium equation in Eq. (30), the coupled nanodisk–substrate problem is reduced to the following single-field sixth-order differential equation in terms of $U\left(r\right)$:

$$
\begin{aligned}
&-l_c^2 l_s^2 \frac{d^6U(r)}{dr^6} - \frac{2l_c^2 l_s^2}{r}\frac{d^5U(r)}{dr^5} \\
&+\left(l_c^2 + l_s^2 + \frac{(5+2\nu)l_c^2 l_s^2}{r^2}\right)\frac{d^4U(r)}{dr^4} + \left(\frac{2l_c^2 + l_s^2}{r} - \frac{(9+10\nu)l_c^2 l_s^2}{r^3}\right)\frac{d^3U(r)}{dr^3} \\
&+\left(-1 - \frac{(1+2\nu)l_c^2 + 3l_s^2}{r^2} + \frac{13(1+2\nu)l_c^2 l_s^2}{r^4}\right)\frac{d^2U(r)}{dr^2} \\
&+\left(-\frac{1}{r} + \frac{(1+2\nu)l_c^2 + 6l_s^2}{r^3} - \frac{20(1+2\nu)l_c^2 l_s^2}{r^5}\right)\frac{dU(r)}{dr} \\
&+\left(\frac{1}{r^2} - \frac{(1+2\nu)l_c^2 + 6l_s^2}{r^4} + \frac{20(1+2\nu)l_c^2 l_s^2}{r^6} + \frac{(1-\nu^2)k_s}{E}\right)U(r) \\
&= \frac{(1-\nu^2)\rho\omega^2}{E} r
\end{aligned}
\tag{31}
$$

2.3.5. Boundary conditions

The sixth-order single-field formulation derived in the preceding section requires six independent boundary conditions. These boundary conditions have two conceptually distinct origins. The first four are mechanical boundary conditions associated with the fourth-order simplified strain-gradient equilibrium of the nanodisk. The remaining two are foundation constitutive boundary conditions arising from the differential representation of the displacement-driven nonlocal foundation. These constitutive conditions are required to preserve the equivalence between the original convolution-type substrate law and its differential counterpart. It can be derived from Eq. (29) as follows:

Classical boundary conditions:

$$
\begin{aligned}
P_1 &= -\frac{Er}{1-\nu^2}\left[\begin{array}{l}\dfrac{dU(r)}{dr} + \nu\dfrac{U(r)}{r} \\ -l_c^2\left(\dfrac{d^3U(r)}{dr^3} + \dfrac{1}{r}\dfrac{d^2U(r)}{dr^2} - \dfrac{1+\nu}{r^2}\dfrac{dU(r)}{dr} + \dfrac{1+\nu}{r^3}U(r)\right)\end{array}\right]_{r=r_0}; \\
P_4 &= \frac{Er}{1-\nu^2}\left[\begin{array}{l}\dfrac{dU(r)}{dr} + \nu\dfrac{U(r)}{r} \\ -l_c^2\left(\dfrac{d^3U(r)}{dr^3} + \dfrac{1}{r}\dfrac{d^2U(r)}{dr^2} - \dfrac{1+\nu}{r^2}\dfrac{dU(r)}{dr} + \dfrac{1+\nu}{r^3}U(r)\right)\end{array}\right]_{r=r_1}
\end{aligned}
\tag{32}
$$

Non-classical boundary conditions:

$$
P_2 = -\left[\frac{El_c^2 r}{1-\nu^2}\left(\frac{d^2U(r)}{dr^2} + \frac{\nu}{r}\frac{dU(r)}{dr} - \frac{\nu}{r^2}U(r)\right)\right]_{r=r_0}; P_5 = \left[\frac{El_c^2 r}{1-\nu^2}\left(\frac{d^2U(r)}{dr^2} + \frac{\nu}{r}\frac{dU(r)}{dr} - \frac{\nu}{r^2}U(r)\right)\right]_{r=r_1}
\tag{33}
$$

Foundation boundary conditions:

$$P_3=\left[q_\Omega-L'\left[U\right]-\frac{1}{l_s}\left(q_\Omega r-L_c\left[U\right]\right)\right]_{r=r_0};P_6=\left[q_\Omega-L'\left[U\right]+\frac{1}{l_s}\left(q_\Omega r-L_c\left[U\right]\right)\right]_{r=r_1} \tag{34}$$

where

$$L_c\left[U\right]=l_c^2\frac{d^4U\left(r\right)}{dr^4}+\frac{2l_c^2}{r}\frac{d^3U\left(r\right)}{dr^3}-\left(1+\frac{\left(1+2\nu\right)l_c^2}{r^2}\right)\frac{d^2U\left(r\right)}{dr^2}-\left(\frac{1}{r}-\frac{\left(1+2\nu\right)l_c^2}{r^3}\right)\frac{dU\left(r\right)}{dr}+\left(\frac{1}{r^2}-\frac{\left(1+2\nu\right)l_c^2}{r^4}\right)U\left(r\right) \tag{35}$$

$$q_\Omega=\frac{\left(1-\nu^2\right)\rho\omega^2}{E} \tag{36}$$

2.3.6. Solutions

The governing differential equation obtained for the coupled rotating nanodisk–substrate system is a sixth-order linear nonhomogeneous ordinary differential equation with variable coefficients. Owing to the linearity of Eq. (31), the general solution can be expressed as the sum of homogeneous and particular components:

$$U\left(r\right)=U_h\left(r\right)+U_p\left(r\right) \tag{37}$$

where $U_h\left(r\right)$ satisfies the corresponding homogeneous equation; and $U_p\left(r\right)$ denotes a particular solution induced by the centrifugal loading. The homogeneous equation is given by

$$U_h\left(r\right)=C_1\phi_1\left(r\right)+C_2\phi_2\left(r\right)+C_3\phi_3\left(r\right)+C_4\phi_4\left(r\right)+C_5\phi_5\left(r\right)+C_6\phi_6\left(r\right) \tag{38}$$

where C_1 to C_6 are the integration constants determined from the six prescribed boundary conditions; and $\phi_1\left(r\right)$ to $\phi_6\left(r\right)$ are the basis functions, as are obtained from the Frobenius-type procedure [56].

3. Numerical simulations

To assess the accuracy and predictive capability of the proposed model, as well as the sensitivity of the radial displacement to the governing system parameters, three numerical simulations are performed. The first examines the number of terms required to achieve convergence of the analytical solution. The second validates the proposed formulation against previously published models. The third investigates the sensitivity of the nanodisk radial displacement to the selected system parameters. All simulations are carried out using Mathematica [57]. The material and geometric properties of the nanodisk and the elastic foundation are listed in Table 1.

3.1. Simulation I: Convergence study

To assess the number of terms (n) required in the solution of Eq. (38), a convergence study is performed for a rotating nanodisk embedded in an elastic substrate. The nanodisk is subjected to the angular velocity (ω) of 10^5 rad/s. The material and geometric properties of the nanodisk and substrate are listed in Table 1. The convergence behavior is examined using n = 4, 8, 16, 32, and 64 terms in the solution expansion. The nanodisk is subjected to radially fixed–free boundary conditions together with the corresponding natural higher-order boundary conditions, which are expressed as follows:

At $r=r_0$**:**

$$U\left(r\right)=0;\ \frac{El_c^2r}{1-\nu^2}\left[\frac{d^2U\left(r\right)}{dr^2}+\frac{\nu}{r}\frac{dU\left(r\right)}{dr}-\frac{\nu}{r^2}U\left(r\right)\right]=0;\ \text{and}\ q_\Omega-L'\left[U\right]-\frac{1}{l_s}\left(q_\Omega r-L_c\left[U\right]\right)=0 \tag{39}$$

At $r = r_1$ **:**

$$\frac{Er}{1-\nu^2}\left[\frac{dU(r)}{dr}+\nu\frac{U(r)}{r}-l_c^2\left(\frac{d^3U(r)}{dr^3}+\frac{1}{r}\frac{d^2U(r)}{dr^2}-\frac{1+\nu}{r^2}\frac{dU(r)}{dr}+\frac{1+\nu}{r^3}U(r)\right)\right]=0;$$

$$\frac{El_c^2 r}{1-\nu^2}\left[\frac{d^2U(r)}{dr^2}+\frac{\nu}{r}\frac{dU(r)}{dr}-\frac{\nu}{r^2}U(r)\right]=0 \text{ ; and } q_\Omega - L'[U]+\frac{1}{l_s}\left(q_\Omega r - L_c[U]\right)=0 \tag{40}$$

Table 1: Properties of nanodisk and nanofoundation.

Structure	Property	Value	Unit	Reference
Nanodisk	E	76	GPa	[11]
	ν	0.37		[11]
	ρ	10,491	kg/m^3	[11]
	l_c	1	nm	[11]
	r_0	1	nm	[11]
	r_1	5	nm	[11]
Nanofoundation	k_s	0.1082	nN/nm^3	[58]
	l_s	0.5	nm	[58]

The convergence results in Figure 2 show that the number of retained series terms affects the six response quantities differently. The displacement and Cauchy-stress fields become reasonably stable with 16 terms, whereas a higher truncation order is necessary to resolve the substrate reaction. This distinction is important when selecting the series length for the subsequent simulations.

The radial displacement provides a clear example of the effect of insufficient truncation. At r = 5 nm, the 4- and 8-term approximations yield negative values of −2.44624 x 10^{-5} and −9.70460 x 10^{-5} nm, respectively. Neither approximation reproduces the outward displacement expected under centrifugal loading. With 16 terms, the predicted displacement changes to 2.26027 x 10^{-4} nm, only 2.11% below the 32-term result of 2.30903 x 10^{-4} nm. No further difference is resolved between 32 and 64 terms at the reported precision. The displacement profile in Figure 2(a) therefore becomes stable before the highest truncation level is reached.

The foundation reaction requires closer attention. Figure 2(b) shows that $D_s(r) = k_s U(r)$ at r = 5 nm decreases from 9.08057 x 10^{-3} nN/nm² with 8 terms to 2.03774 x 10^{-4} nN/nm² with 16 terms. The corresponding 32-term value is 1.11228 x 10^{-5} nN/nm². Thus, a series length that gives a displacement difference of approximately 2% can still produce a much larger relative discrepancy in the reaction field. At r = 4 nm, for instance, the 16-term and 32-term reactions are 7.16699 x 10^{-5} and 1.89646 x 10^{-5} nN/nm², respectively. The slow stabilization of $D_s(r)$ is consistent with its evaluation through the differential equilibrium relation, which involves higher derivatives of the displacement. It also indicates that convergence should not be assessed from the displacement alone.

The Cauchy stresses exhibit a more regular convergence pattern, as seen in Figures 2(c) and 2(d). At the inner radius, the radial stress changes from 0.00948588 GPa with 16 terms to 0.00964649 GPa with 32 terms, a difference of 1.66%. The converged distribution decreases across the annulus and reaches 0.00338407 GPa at the outer radius. The circumferential stress follows a different radial profile. Starting from 0.00356920 GPa at the inner boundary, it rises to approximately 0.00684484 GPa near r = 2.5 nm and then decreases to 0.00476183 GPa at r = 5 nm. At the location of the peak, the 16-term approximation differs from the 32-term value by approximately 1.83%. These results show that the conventional stress fields are substantially less sensitive to truncation than the substrate reaction once 16 or more terms are retained.

The double-stress components in Figures 2(e) and 2(f) also approach stable distributions as the series is extended. At r = 3 nm, the radial double stress changes from −2.16211 x 10^{-3} to −2.18041 x 10^{-3} nN/nm between 16 and 32 terms, corresponding to a difference of approximately 0.84%. For the circumferential double stress at the inner radius, the corresponding values are 8.18726 x 10^{-3} and 8.32588 x 10^{-3} nN/nm, giving a difference of 1.66%. These stress measures involve the second derivative of $U(r)$, making their evaluation sensitive to the quality of the underlying series approximation, particularly at low truncation orders.

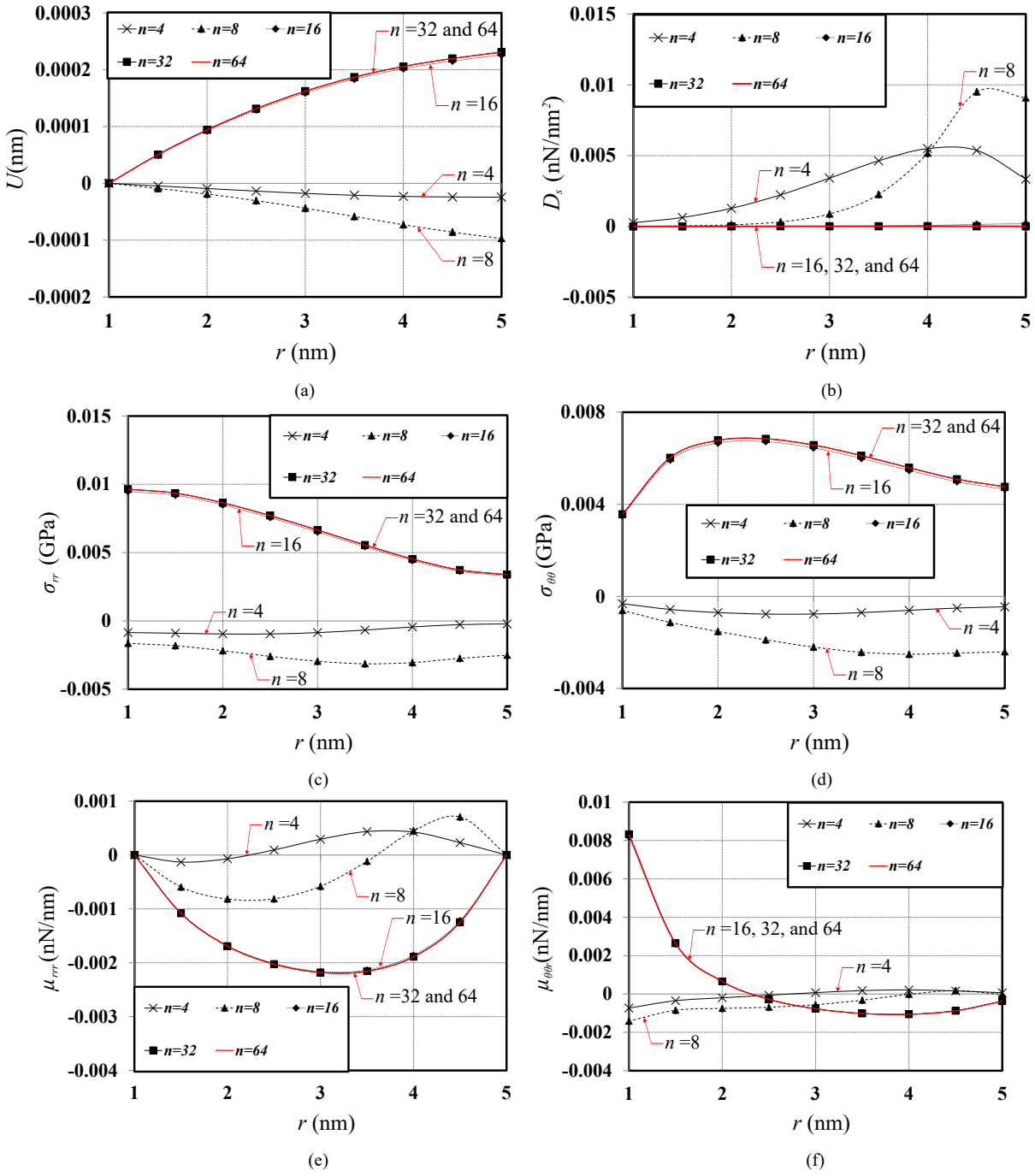


Fig 2: Responses of Simulation I: (a) Radial displacement; (b) Radial substrate reaction; (c) Radial Cauchy stress; (d) Circumferential Cauchy stress; (e) Radial double stress; and (f) Circumferential strain-gradient double stress.

Taken together, the results indicate that 16 terms may be adequate when moderate accuracy in displacement or stress is sufficient, but they are not appropriate for evaluating the complete coupled response. Increasing the truncation order to 32 removes the visible differences relative to the 64-term results for all six quantities examined. The subsequent simulations therefore employ 32 retained terms for the investigated parameter sets.

3.2. Simulation II: Model validation

To assess the accuracy of the proposed formulation, two classical limiting cases are considered and compared with finite element (FE) solutions: a classical rotating nanodisk embedded in an elastic substrate and a classical rotating nanodisk without substrate restraint. The first case is obtained by suppressing the material length-scale

effects while retaining the elastic substrate, whereas the second is obtained by suppressing both the material length-scale effects and the substrate stiffness. The nanodisk rotates with an angular velocity of $\omega = 10^4$ rad/s. The material and geometric properties of the nanodisk and substrate are listed in Table 1. Radially fixed–free boundary conditions are imposed together with the corresponding natural higher-order boundary conditions, as defined in Eqs. (39) and (40). For independent verification, the two classical limiting cases are reproduced using ABAQUS [59]. The rotating annular disk is modeled axisymmetrically and discretized using four-node bilinear axisymmetric quadrilateral elements with reduced integration (CAX4R), as presented in Figure 3.

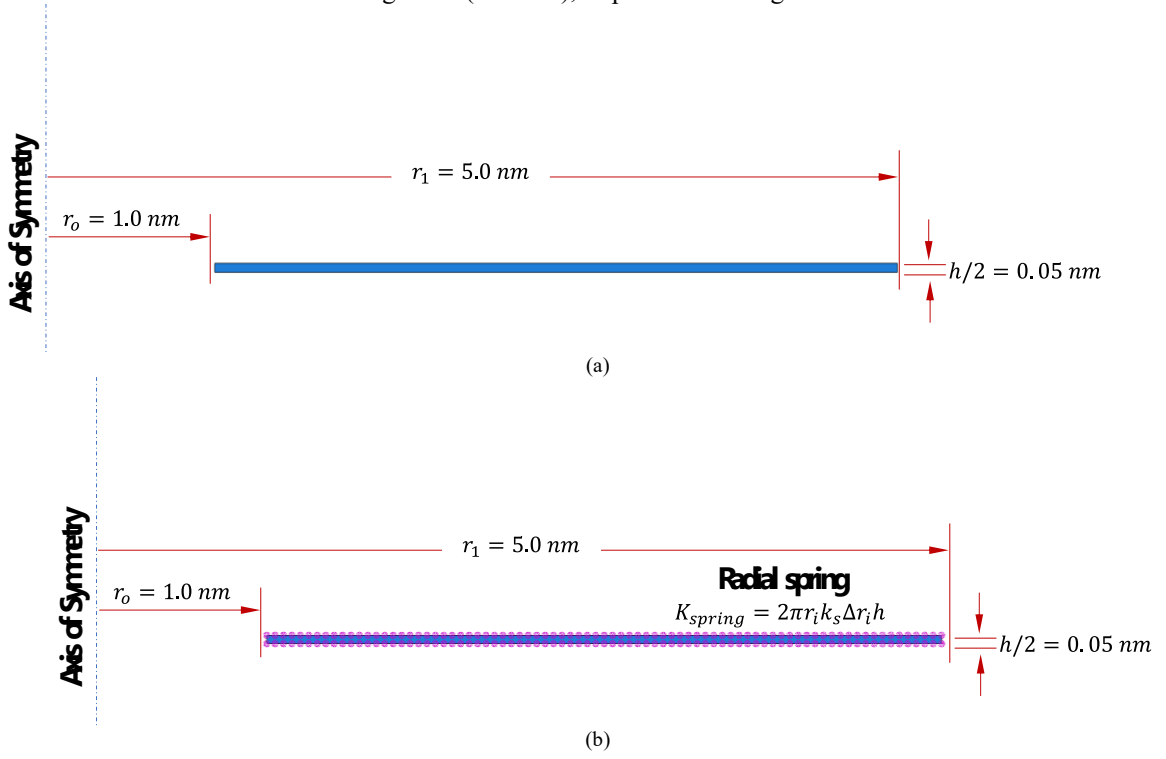


Fig 3: FE model for: (a) Classical rotating nanodisk without substrate restraint; and (b) Classical rotating nanodisk embedded in an elastic substrate.

The comparison in Figure 4 examines whether the analytical formulation reproduces the classical rotating-disk response when the strain-gradient contribution is removed. Two reference configurations are considered: an unsupported annular disk and a disk restrained by a local Winkler foundation. Both are analyzed under radially fixed–free boundary conditions and compared with ABAQUS finite element (FE) solutions. The comparison is restricted to these classical limiting cases rather than the complete strain-gradient nonlocal model.

For radial displacement, the agreement is particularly close. At the outer radius, the unsupported disk gives 2.41180 x 10^{-4} nm analytically and 2.41211 x 10^{-4} nm in the FE model. The difference is approximately 0.013%. The corresponding values for the foundation-supported disk are 2.27519 x 10^{-4} and 2.27547 x 10^{-4} nm, differing by approximately 0.012%. The nearly overlapping curves in Figure 4(a) are therefore supported by the numerical values rather than being only a visual observation. Comparing the two analytical solutions also shows that the Winkler foundation reduces the outer-radius expansion by 5.66%.

The radial stress comparison reveals a different feature of the numerical agreement. At the restrained inner boundary, the analytical stress is 15.0217 MPa without the foundation and 14.1653 MPa with it. ABAQUS predicts 14.7758 and 13.9322 MPa, respectively. These differences are approximately 1.64–1.65%, substantially larger than those obtained for displacement. The agreement improves away from the boundary: at $r = 3$ nm, the analytical and FE values are 7.2765 and 7.2770 MPa for the unsupported disk, while the supported disk gives 6.8635 and 6.8640 MPa. The differences at this location are below 0.01%. Figure 4(b) therefore suggests that the remaining disagreement is concentrated mainly near the disk boundaries rather than distributed throughout the annulus.

A similar pattern appears in the circumferential stress response. Both methods predict an increase from the inner boundary to a peak within the annular domain, followed by a decrease toward the outer edge. At $r = 2$ nm, the unsupported disk gives 8.3536 MPa analytically and 8.3533 MPa from FE analysis. With foundation restraint, these

values decrease to 7.8661 and 7.8658 MPa. The analytical–FE differences at this location are approximately 0.003–0.004%, while the foundation itself reduces the circumferential stress by 5.84%. At the outer radius, the analytical stress falls from 3.6659 MPa without the substrate to 3.4583 MPa with the substrate, a reduction of 5.66%.

The agreement is less exact at the boundaries, where stress recovery and discretization can influence the FE predictions. The largest reported relative discrepancies near the inner edge are approximately 1.65% for radial stress and 3.93% for circumferential stress. A small nonzero radial stress also remains in the FE output at the analytically traction-free outer edge. These differences do not establish an error in either solution, but their source cannot be identified conclusively without a mesh-sensitivity assessment and examination of the stress-extraction procedure. Within the classical cases examined, the analytical and FE predictions show close agreement, particularly for displacement and stresses away from the boundaries. The comparison also indicates that local foundation restraint lowers centrifugal expansion and conventional stresses by approximately 5–6% for the selected parameters. These results provide a reference for assessing the additional effects of material strain-gradient elasticity and foundation nonlocality in Simulation III.

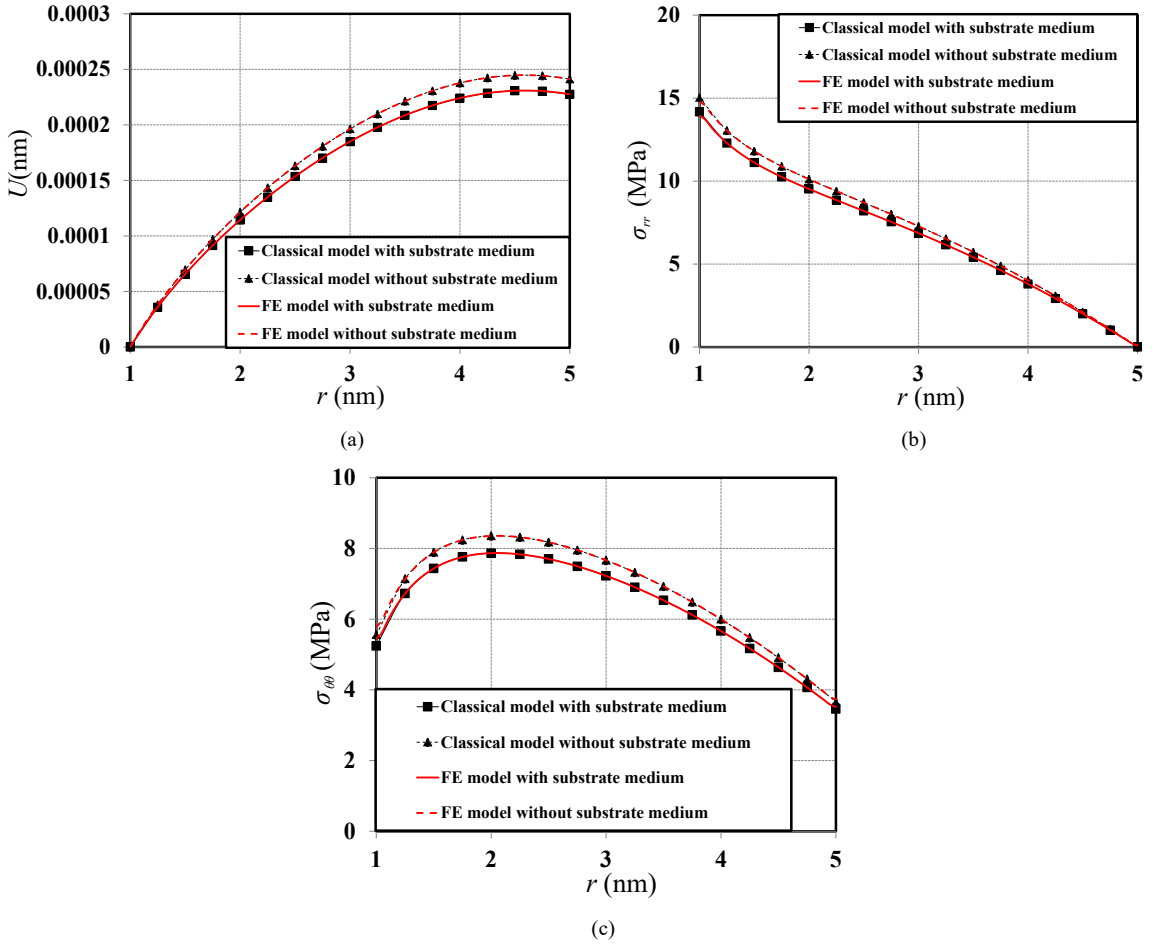


Fig 4: Responses of Simulation II: (a) Radial displacement; (b) Radial Cauchy stress; and (c) Circumferential Cauchy stress.

3.3. Simulation III: Parametric studies

To investigate the sensitivity of the radial displacement of a rotating nanodisk embedded in an elastic substrate to the selected system parameters, the nanodisk is assumed to rotate at an angular velocity of $\omega = 10^5$ rad/s. The material and geometric properties of the nanodisk and substrate are listed in Table 1. Radially fixed–free boundary conditions are imposed together with the corresponding natural higher-order boundary conditions, as defined in Eqs. (39) and (40). The parameters considered in the sensitivity analysis are the nondimensional material length-scale parameter ($0 \le \xi_c = l_c / r_0 \le 2$), the nondimensional nonlocal substrate parameter ($0 \le \xi_s = l_s / r_0 \le 2$), and the

nondimensional substrate stiffness ($\bar{K}_s = k_s / Er_0$ = 0.01, 0.05, and 0.1).

Figure 5 illustrates the coupled effects of the nondimensional material length-scale parameter (ξ_c), foundation nonlocal length-scale parameter (ξ_s), and substrate stiffness ($\bar{K}_s$) on the radial displacement of the rotating annular nanodisk. Three substrate stiffness levels, $\bar{K}_s$ = 0.01, 0.05, and 0.1, are considered in Figures 5(a)–(c), respectively, while both characteristic length-scale parameters vary from 0 to 2. The results show that material strain-gradient elasticity and foundation nonlocality exert competing influences on the centrifugal deformation, with their relative importance depending strongly on the substrate stiffness.

As shown in Figure 5(a), increasing ξ_c generally reduces the radial displacement, indicating the stiffening effect associated with strain-gradient elasticity. For $\bar{K}_s = 0.01$ and $\xi_s = 0$, the displacement decreases from 2.31418 x 10^{-4} nm at $\xi_c = 0$ to 2.09226 x 10^{-4} nm at $\xi_c = 2$, corresponding to a reduction of approximately 9.59%. A similar trend is observed when foundation nonlocality is present. At $\xi_s = 2$, increasing ξ_c from 0 to 2 reduces the displacement from 2.36328 x 10^{-4} to 2.12829 x 10^{-4} nm, a decrease of approximately 9.94%. By contrast, increasing ξ_s produces a larger radial displacement. At $\xi_c = 0$, increasing ξ_s from 0 to 2 increases the displacement by approximately 2.12%, indicating that foundation nonlocality has only a modest influence when the substrate is relatively compliant.

The interaction becomes more pronounced at the intermediate stiffness ($\bar{K}_s = 0.05$), as shown in Figure 5(b). In the local-foundation limit ($\xi_s = 0$), increasing ξ_c from 0 to 2 reduces the displacement from 2.01069 x 10^{-4} to 1.86100 x 10^{-4} nm, corresponding to a decrease of approximately 7.44%. In contrast, for $\xi_c = 0$, increasing ξ_s from 0 to 2 raises the displacement from 2.01069 x 10^{-4} to 2.18807 x 10^{-4} nm, an increase of approximately 8.82%. At $\xi_c = 2$, the corresponding increase is approximately 8.10%. Compared with the results for $\bar{K}_s = 0.01$, the displacement therefore becomes more sensitive to the foundation nonlocal length scale as the substrate stiffness increases.

Figure 5(c) shows the response for $\bar{K}_s = 0.1$. Under the local-foundation condition ($\xi_s = 0$), increasing ξ_c from 0 to 2 reduces the displacement from 1.69822 x 10^{-4} to 1.63504 x 10^{-4} nm, corresponding to a reduction of approximately 3.72%. This reduction is smaller than those obtained for the lower substrate stiffnesses. By contrast, the effect of foundation nonlocality becomes markedly stronger. For $\xi_c = 0$, increasing ξ_s from 0 to 2 increases the displacement from 1.69822 x 10^{-4} to 2.00397 x 10^{-4} nm, an increase of approximately 18.00%. Even at $\xi_c = 2$, the corresponding increase remains approximately 15.16%. These results indicate that foundation nonlocality becomes increasingly influential as the substrate stiffness increases.

The effect of $\bar{K}_s$ can also be assessed by comparing Figures 5(a)–(c) at fixed characteristic length scales. In the classical local limit ($\xi_c = \xi_s = 0$), increasing $\bar{K}_s$ from 0.01 to 0.1 reduces the radial displacement from 2.31418 x 10^{-4} to 1.69822 x 10^{-4} nm, corresponding to a reduction of approximately 26.62%. When $\xi_c = 0$ and $\xi_s = 2$, however, the corresponding reduction is only approximately 15.20%, from 2.36328 x 10^{-4} to 2.00397 x 10^{-4} nm. This comparison indicates that the restraining effect of the substrate depends not only on its nominal stiffness but also on the characteristic length governing the nonlocal foundation response. Within the adopted displacement-driven formulation, increasing ξ_s redistributes the substrate reaction over a larger interaction domain, thereby reducing the effective radial restraint for the displacement fields considered here.

Overall, the results show that the material and foundation length-scale effects act in opposite directions. A larger material characteristic length reduces centrifugal expansion, whereas a larger foundation nonlocal length increases the radial displacement under the conditions considered. As the substrate becomes stiffer, the effect of the material length scale becomes less evident, while the influence of foundation nonlocality becomes more pronounced. The two characteristic lengths should therefore be considered separately when evaluating the response of rotating nanodisks supported by elastic media. In particular, neglecting foundation nonlocality may lead to an overestimation of the radial restraint provided by a relatively stiff substrate.

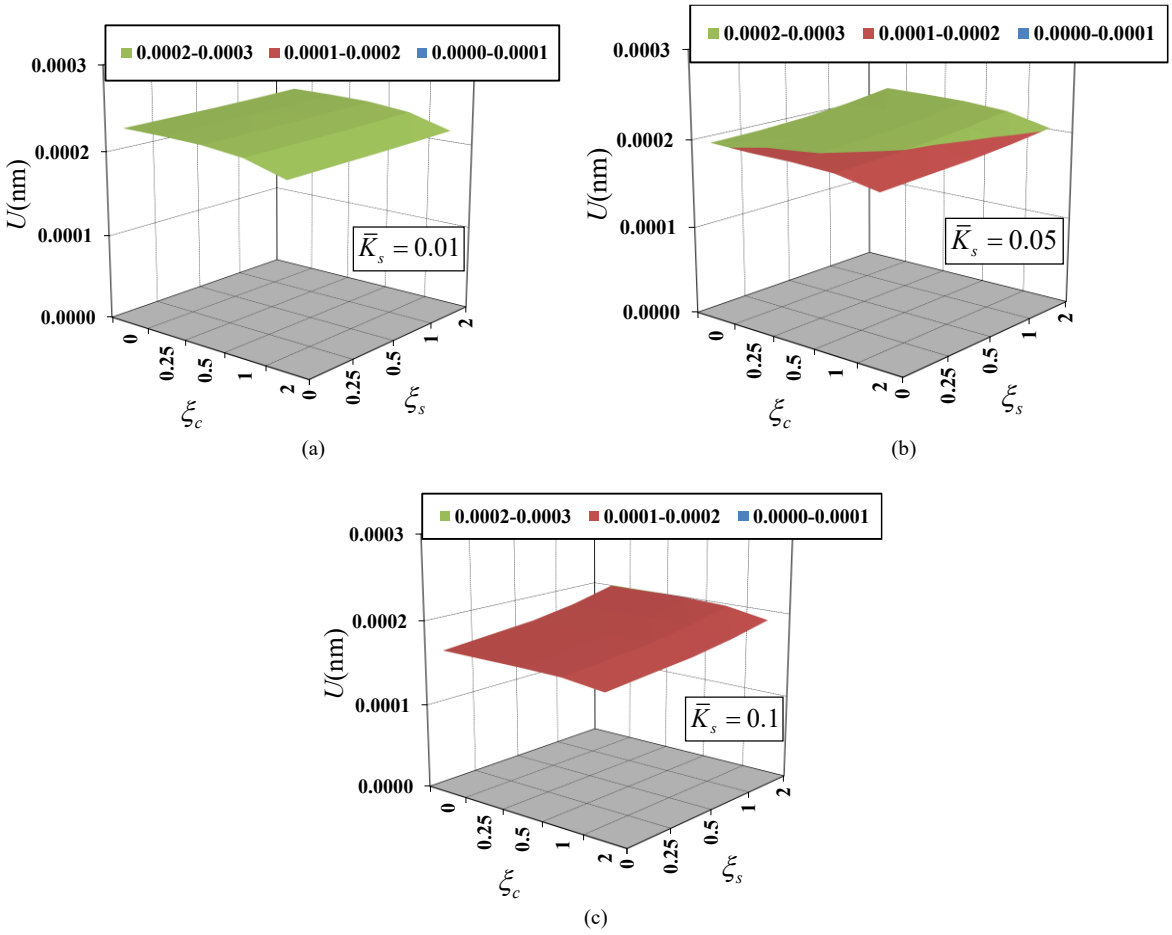


Fig 5: Radial displacement with variation of non-dimensional material length-scale parameter, nonlocal substrate medium parameter, and substrate medium stiffness of: (a) $\bar{K}_s = 0.01$; (b) $\bar{K}_s = 0.05$; and (c) $\bar{K}_s = 0.1$.

4. Conclusion

This study developed a displacement-based analytical formulation for the axisymmetric centrifugal response of a strain-gradient rotating annular nanodisk interacting with a displacement-driven nonlocal elastic foundation. Material small-scale effects were incorporated through a one-parameter simplified strain-gradient theory, while substrate nonlocality was represented by a bi-exponential attenuation kernel. By combining the variational equilibrium relation with the differential constitutive equation of the foundation, the coupled problem was reduced to a sixth-order governing differential equation supplemented by four mechanical and two foundation constitutive boundary conditions. A Frobenius-type series solution was then constructed. The principal findings are summarized as follows:

- The number of series terms needed for a stable result depends on the response quantity. With 16 terms, the radial displacement and stress measures are relatively close to their converged values, but the substrate reaction still shows considerable differences. Extending the series to 32 terms produces results that coincide with those obtained using 64 terms at the reported precision. This makes 32 retained terms an appropriate choice for the parameter sets examined.
- The classical limiting solutions agree closely with finite element calculations for annular disks with and without local Winkler restraint. At the outer radius, the analytical–FE displacement differences are approximately 0.013% for the unsupported disk and 0.012% for the supported disk. Stress predictions also agree well within the annular domain, although larger differences occur near the boundaries. The comparison verifies the classical limits of the formulation; the fully coupled strain-gradient nonlocal case remains outside the scope of this FE benchmark.
- Material strain-gradient elasticity tends to restrict centrifugal expansion. For a local foundation, increasing the nondimensional material length-scale parameter from 0 to 2 reduces radial displacement by 9.59%,

7.44%, and 3.72% at substrate stiffness parameters of 0.01, 0.05, and 0.1, respectively. The smaller percentage reduction at higher substrate stiffness indicates that the relative contribution of material strain-gradient stiffening decreases as the restraint provided by the foundation becomes stronger.

- Foundation nonlocality produces the opposite displacement trend over the investigated range. With the material length-scale parameter set to zero, increasing the foundation nonlocal parameter from 0 to 2 raises radial displacement by 2.12%, 8.82%, and 18.00% for the three substrate stiffness levels. The effect is therefore most pronounced for the stiffest foundation considered. In the present model, a larger nonlocal interaction length reduces the effective restraint relative to the corresponding local foundation.
- The displacement reduction achieved by increasing substrate stiffness depends on the nonlocal interaction length. When both characteristic length-scale parameters are zero, increasing the substrate stiffness parameter from 0.01 to 0.1 reduces displacement by 26.62%. For a foundation nonlocal parameter of 2 and a zero material length-scale parameter, the reduction is only 15.20%. Substrate stiffness and its nonlocal interaction length must therefore be considered together when evaluating centrifugal deformation.

The results indicate that material strain-gradient elasticity and displacement-driven foundation nonlocality cannot be treated as interchangeable size effects. Their contributions oppose one another under the conditions studied, and the balance between them changes with substrate stiffness. The analysis is limited to one-dimensional radial strain gradients and a radial representation of the nonlocal foundation. Extensions to full cylindrical strain-gradient kinematics, two-dimensional substrate interactions, and temperature-dependent material behavior would help establish the applicability of the model to more general rotating nanostructures.

Acknowledgements

This research was supported by University of Phayao and the Fundamental Fund (FF) 2027 (Grant No. 2374/2569) under Thailand RISE Fund, awarded to W. Sae-Long, by National Research Council of Thailand (NRCT) and KMUTNB under the Senior Research Scholar program (Contract No. N42A690479), awarded to P. Sukontasukkul, and by University of Phayao and the Fundamental Fund (FF) 2027 (Grant No. 2284/2569) under Thailand RISE Fund, awarded to N. Damrongwiriyanupap.

References

[1] H.-H. Lin, A. Croy, R. Gutierrez, C. Joachim, G. Cuniberti, A nanographene disk rotating a single molecule gear on a Cu(111) surface, *Nanotechnology,* Vol. 33, No. 17, 2022.

[2] A. Alizadeh, M. Shishehsaz, S. Shahrooi, A. Reza, Free vibration characteristics of viscoelastic nano-disks based on modified couple stress theory, *The Journal of Strain Analysis for Engineering Design,* Vol. 58, No. 4, pp. 270-296, 2023.

[3] A. E. Oke, A. F. Kineber, O. Akindele, D. Ekundayo, Determining the stationary barriers to the implementation of radio frequency identification (RFID) technology in an emerging construction industry, *Journal of Engineering, Design and Technology,* Vol. 22, No. 6, pp. 1894-1912, 2023.

[4] Z. Ying, Z. Wang, Z. Zhao, S. Dhar, D. Z. Pan, R. Soref, R. T. Chen, Comparison of microrings and microdisks for high-speed optical modulation in silicon photonics, *Applied Physics Letters,* Vol. 112, No. 11, 2018.

[5] V. Danesh, M. Asghari, Analysis of micro-rotating disks based on the strain gradient elasticity, *Acta Mechanica,* Vol. 225, No. 7, pp. 1955-1965, 2014/07/01, 2014.

[6] M. Baghani, N. Heydarzadeh, M. M. Roozbahani, Stress Analysis of a Functionally Graded Micro/ Nanorotating Disk with Variable Thickness Based on the Strain Gradient Theory, *International Journal of Applied Mechanics,* Vol. 08, No. 02, pp. 1650020, 2016.

[7] M. Hosseini, M. Shishesaz, K. N. Tahan, A. Hadi, Stress analysis of rotating nano-disks of variable thickness made of functionally graded materials, *International Journal of Engineering Science,* Vol. 109, pp. 29-53, 2016/12/01/, 2016.

[8] M. Shishesaz, M. Hosseini, K. Naderan Tahan, A. Hadi, Analysis of functionally graded nanodisks under thermoelastic loading based on the strain gradient theory, *Acta Mechanica,* Vol. 228, No. 12, pp. 4141-4168, 2017/12/01, 2017.

[9] M. Hosseini, M. Shishesaz, A. Hadi, Thermoelastic analysis of rotating functionally graded micro/nanodisks of variable thickness, *Thin-Walled Structures,* Vol. 134, pp. 508-523, 2019/01/01/, 2019.

[10] E. Bagheri, M. Asghari, V. Danesh, Analytical study of micro-rotating disks with angular acceleration on the basis of the strain gradient elasticity, *Acta Mechanica,* Vol. 230, No. 9, pp. 3259-3278, 2019/09/01, 2019.

[11] A. Barati, M. Mousavi Khoram, M. Shishesaz, M. Hosseini, Size-dependent thermoelastic analysis of rotating nanodisks of variable thickness, *Journal of Computational Applied Mechanics,* Vol. 51, No. 2, pp. 340-360, 2020. en

[12] E. Bagheri, M. Asghari, A. Kargarzadeh, M. Badiee, Small-scale oriented elasticity modeling of functionally graded rotating micro-disks with varying angular velocity in the context of the strain gradient theory, *Acta Mechanica,* Vol. 232, No. 6, pp. 2395-2416, 2021/06/01, 2021.

[13] M. S. H. Al-Furjan, R. Dehini, M. Khorami, M. Habibi, D. won Jung, On the dynamics of the ultra-fast rotating cantilever orthotropic piezoelectric nanodisk based on nonlocal strain gradient theory, *Composite Structures,* Vol. 255, pp. 112990, 2021/01/01/, 2021.

[14] J. Guo, A. Baharvand, D. Tazeddinova, M. Habibi, H. Safarpour, A. Roco-Videla, A. Selmi, An intelligent computer method for vibration responses of the spinning multi-layer symmetric nanosystem using multi-physics modeling, *Engineering with Computers,* Vol. 38, No. 5, pp. 4217-4238, 2022/12/01, 2022.

[15] R. Panahi, M. Asghari, V. Borjalilou, Nonlinear forced vibration analysis of micro-rotating shaft–disk systems through a formulation based on the nonlocal strain gradient theory, *Archives of Civil and Mechanical Engineering,* Vol. 23, No. 2, pp. 85, 2023/02/22, 2023.

[16] R. D. Mindlin, Micro-structure in linear elasticity, *Archive for Rational Mechanics and Analysis,* Vol. 16, No. 1, pp. 51-78, 1964/01/01, 1964.

[17] R. D. Mindlin, N. N. Eshel, On first strain-gradient theories in linear elasticity, *International Journal of Solids and Structures,* Vol. 4, No. 1, pp. 109-124, 1968/01/01/, 1968.

[18] B. S. Altan, E. C. Aifantis, On Some Aspects in the Special Theory of Gradient Elasticity*,* Vol. 8, No. 3, pp. 231-282, 1997.

[19] E. C. Aifantis, Strain gradient interpretation of size effects, *International Journal of Fracture,* Vol. 95, No. 1, pp. 299-314, 1999/01/01, 1999.

[20] F. Yang, A. C. M. Chong, D. C. C. Lam, P. Tong, Couple stress based strain gradient theory for elasticity, *International Journal of Solids and Structures,* Vol. 39, No. 10, pp. 2731-2743, 2002/05/01/, 2002.

[21] D. C. C. Lam, F. Yang, A. C. M. Chong, J. Wang, P. Tong, Experiments and theory in strain gradient elasticity, *Journal of the Mechanics and Physics of Solids,* Vol. 51, No. 8, pp. 1477-1508, 2003/08/01/, 2003.

[22] X. L. Gao, S. K. Park, Variational formulation of a simplified strain gradient elasticity theory and its application to a pressurized thick-walled cylinder problem, *International Journal of Solids and Structures,* Vol. 44, No. 22, pp. 7486-7499, 2007/11/01/, 2007.

[23] H. Askes, E. C. Aifantis, Gradient elasticity in statics and dynamics: An overview of formulations, length scale identification procedures, finite element implementations and new results, *International Journal of Solids and Structures,* Vol. 48, No. 13, pp. 1962-1990, 2011/06/15/, 2011.

[24] B. Akgöz, Ö. Civalek, Strain gradient elasticity and modified couple stress models for buckling analysis of axially loaded micro-scaled beams, *International Journal of Engineering Science,* Vol. 49, No. 11, pp. 1268-1280, 2011/11/01/, 2011.

[25] E. Benvenuti, A. Simone, One-dimensional nonlocal and gradient elasticity: Closed-form solution and size effect, *Mechanics Research Communications,* Vol. 48, pp. 46-51, 2013/03/01/, 2013.

[26] X. Liang, S. Hu, S. Shen, A new Bernoulli–Euler beam model based on a simplified strain gradient elasticity theory and its applications, *Composite Structures,* Vol. 111, pp. 317-323, 2014/05/01/, 2014.

[27] B. Akgöz, Ö. Civalek, Longitudinal vibration analysis for microbars based on strain gradient elasticity theory, *Journal of Vibration and Control,* Vol. 20, No. 4, pp. 606-616, 2014/03/01, 2014.

[28] B. Akgöz, Ö. Civalek, Bending analysis of FG microbeams resting on Winkler elastic foundation via strain gradient elasticity, *Composite Structures,* Vol. 134, pp. 294-301, 2015/12/15/, 2015.

[29] L. Li, X. Li, Y. Hu, Free vibration analysis of nonlocal strain gradient beams made of functionally graded material, *International Journal of Engineering Science,* Vol. 102, pp. 77-92, 2016/05/01/, 2016.

[30] G. Fu, S. Zhou, L. Qi, On the strain gradient elasticity theory for isotropic materials, *International Journal of Engineering Science,* Vol. 154, pp. 103348, 2020/09/01/, 2020.

[31] L. Lu, X. Guo, J. Zhao, A unified nonlocal strain gradient model for nanobeams and the importance of higher order terms, *International Journal of Engineering Science,* Vol. 119, pp. 265-277, 2017/10/01/, 2017.

[32] L. Lu, X. Guo, J. Zhao, Size-dependent vibration analysis of nanobeams based on the nonlocal strain gradient theory, *International Journal of Engineering Science,* Vol. 116, pp. 12-24, 2017/07/01/, 2017.

[33] S. Limkatanyu, N. Damrongwiriyanupap, W. Prachasaree, W. Sae-Long, Modeling of axially loaded nanowires embedded in elastic substrate media with inclusion of nonlocal and surface effects, *Journal of Nanomaterials,* Vol. 2013, pp. 104, 2013.

[34] C. Demir, K. Mercan, H. M. Numanoglu, O. Civalek, Bending Response of Nanobeams Resting on Elastic Foundation, *Journal of Applied and Computational Mechanics,* Vol. 4, No. 2, pp. 105-114, 2018. en

[35] S. Limkatanyu, W. Sae-Long, S. Horpibulsuk, W. Prachasaree, N. Damrongwiriyanupap, Flexural responses of nanobeams with coupled effects of nonlocality and surface energy, *ZAMM - Journal of Applied Mathematics and Mechanics / Zeitschrift für Angewandte Mathematik und Mechanik,* Vol. 98, No. 10, pp. 1771-1793, 2018/10/01, 2018.

[36] P. Ponbunyanon, S. Limkatanyu, W. Kaewjuea, W. Prachasaree, T. Chub-Uppakarn, A Novel Beam-Elastic Substrate Model with Inclusion of Nonlocal Elasticity and Surface Energy Effects, *Arabian Journal for Science and Engineering,* Vol. 41, No. 10, pp. 4099-4113, 2016/10/01, 2016.

[37] W. Sae-Long, S. Limkatanyu, W. Prachasaree, J. Rungamornrat, P. Sukontasukkul, A Thermodynamics-Based Nonlocal Bar-Elastic Substrate Model with Inclusion of Surface-Energy Effect, *Journal of Nanomaterials,* Vol. 2020, No. 1, pp. 8276745, 2020/01/01, 2020.

[38] W. Sae-Long, S. Limkatanyu, J. Rungamornrat, W. Prachasaree, P. Sukontasukkul, H. M. Sedighi, A rational beam-elastic substrate model with incorporation of beam-bulk nonlocality and surface-free energy, *The European Physical Journal Plus,* Vol. 136, No. 1, pp. 80, 2021/01/13, 2021.

[39] W. Sae-Long, S. Limkatanyu, P. Sukontasukkul, N. Damrongwiriyanupap, J. Rungamornrat, W. Prachasaree, FOURTH-ORDER STRAIN GRADIENT BAR-SUBSTRATE MODEL WITH NONLOCAL AND SURFACE EFFECTS FOR THE ANALYSIS OF NANOWIRES EMBEDDED IN SUBSTRATE MEDIA, *Facta Universitatis, Series: Mechanical Engineering; Vol 19, No 4 (2021)DO - 10.22190/FUME201009045S*, 12/12/, 2021.

[40] S. Limkatanyu, W. Sae-Long, H. Mohammad-Sedighi, J. Rungamornrat, P. Sukontasukkul, T. Imjai, H. Zhang, Static and Free Vibration Analyses of Single-Walled Carbon Nanotube (SWCNT)–Substrate Medium Systems, *Nanomaterials,* 12, 2022].

[41] S. Limkatanyu, W. Sae-Long, H. Mohammad-Sedighi, J. Rungamornrat, P. Sukontasukkul, W. Prachasaree, T. Imjai, Strain-Gradient Bar-Elastic Substrate Model with Surface-Energy Effect: Virtual-Force Approach, *Nanomaterials,* 12, 2022].

[42] T. Luo, Q. Mao, S. Zeng, K. Wang, B. Wang, J. Wu, Z. Lu, Scale Effect on the Nonlinear Vibration of Piezoelectric Sandwich Nanobeams on Winkler Foundation, *Journal of Vibration Engineering & Technologies,* Vol. 9, No. 6, pp. 1289-1303, 2021/09/01, 2021.

[43] S. Karmakar, S. Chakraverty, Thermal vibration of nonhomogeneous Euler nanobeam resting on Winkler foundation, *Engineering Analysis with Boundary Elements,* Vol. 140, pp. 581-591, 2022/07/01/, 2022.

[44] Y.-f. Zheng, D.-y. Qu, L.-c. Liu, C.-p. Chen, Size-dependent nonlinear bending analysis of nonlocal magneto-electro-elastic laminated nanobeams resting on elastic foundation, *International Journal of Non-Linear Mechanics,* Vol. 148, pp. 104255, 2023/01/01/, 2023.

[45] S. Limkatanyu, W. Sae-Long, J. Rungamornrat, N. Damrongwiriyanupap, S. Keawsawasvong, P. Sukontasukkul, C. Hansapinyo, Static Bending Analysis of Nanobeam-Substrate Medium Systems Incorporating Mixture Stress-Driven Nonlocality, Surface Energy, and Substrate-Structure Interactions, *Journal of Applied and Computational Mechanics,* Vol. 11, No. 2, pp. 327-343, 2025. en

[46] W. Sae-Long, S. Limkatanyu, P. Sukontasukkul, J. Rungamornrat, S. Keawsawasvong, T. Chompoorat, P. Chaimahawan, A. Pimanmas, Nonlocal Static and Dynamic Characterization of Nanobeams on Elastic Substrates with Surface Energy Effects, *Journal of Applied and Computational Mechanics,* Vol. 12, No. 3, pp. 1217-1232, 2026. en

[47] A. A. León Baldelli, B. Bourdin, On the Asymptotic Derivation of Winkler-Type Energies from 3D Elasticity, *Journal of Elasticity,* Vol. 121, No. 2, pp. 275-301, 2015/12/01, 2015.

[48] A. C. Eringen, D. G. B. Edelen, On nonlocal elasticity, *International Journal of Engineering Science,* Vol. 10, No. 3, pp. 233-248, 1972/03/01/, 1972.

[49] J. Peddieson, G. R. Buchanan, R. P. McNitt, Application of nonlocal continuum models to nanotechnology, *International Journal of Engineering Science,* Vol. 41, No. 3, pp. 305-312, 2003/03/01/, 2003.

[50] J. Fernández-Sáez, R. Zaera, J. A. Loya, J. N. Reddy, Bending of Euler–Bernoulli beams using Eringen's integral formulation: A paradox resolved, *International Journal of Engineering Science,* Vol. 99, pp. 107-116, 2016/02/01/, 2016.

[51] G. Romano, R. Barretta, M. Diaco, F. Marotti de Sciarra, Constitutive boundary conditions and paradoxes in nonlocal elastic nanobeams, *International Journal of Mechanical Sciences,* Vol. 121, pp. 151-156, 2017/02/01/, 2017.

[52] M. I. Friswell, S. Adhikari, Y. Lei, Vibration analysis of beams with non-local foundations using the finite element method, *International Journal for Numerical Methods in Engineering,* Vol. 71, No. 11, pp. 1365-1386, 2007/09/10, 2007.

[53] V. D. Potapov, On bending and stability of beams and plates laying on a continuous nonlocally elastic foundation, *Journal of Machinery Manufacture and Reliability,* Vol. 45, No. 3, pp. 199-205, 2016/05/01, 2016.

[54] M. S. Vaccaro, F. P. Pinnola, F. Marotti de Sciarra, R. Barretta, Elastostatics of Bernoulli–Euler Beams Resting on Displacement-Driven Nonlocal Foundation, *Nanomaterials,* 11, 2021].

[55] R. Barretta, M. Čanađija, R. Luciano, F. Marotti de Sciarra, On the mechanics of nanobeams on nano-foundations, *International Journal of Engineering Science,* Vol. 180, pp. 103747, 2022/10/01/, 2022.

[56] S. Arun, M. O. T. Cole, C. Chamroon, W. Fakkaew, Geometry-Parametrized Stress Solution for the Rotating Conical Disk with Application to Rotor Design Optimization, *International Journal of Applied Mechanics,* Vol. 18, No. 05, pp. 2650024, 2026/05/01, 2026.

[57] S. Wolfram, 1992, *Mathematica: A System for Doing Mathematics by Computer*, Addison-Wesley Publishing Company, Redwood City, California

[58] B. Das, D. Ussorio, M. S. Vaccaro, R. Barretta, R. Luciano, Dynamics of FG nanobeams on nonlocal medium, *Composite Structures,* Vol. 366, pp. 119057, 2025/08/15/, 2025.

[59] S. Dassault Systèmes, 2021, *Abaqus Documentation (Version 2021-EF)*, Dassault Systèmes SIMULIA Corp.,